

ARTICLE OPEN



Rabenosyn-5 suppresses non-small cell lung cancer metastasis via inhibiting CDC42 activity

Xiong Guo¹, Bin Mu², Lin Zhu^{3,4}, Yanli Zhuo⁵, Ping Mu^{4,6}, Fu Ren^{4,7} and Fangjin Lu^{8,9}

© The Author(s) 2024

Metastasis, the primary cause of death in lung cancer patients, is facilitated by cytoskeleton remodeling, which plays a crucial role in cancer cell migration and invasion. However, the precise regulatory mechanisms of intracellular trafficking proteins involved in cytoskeleton remodeling remain unclear. In this study, we have identified Rabenosyn-5 (Rbsn) as an inhibitor of filopodia formation and lung cancer metastasis. Mechanistically, Rbsn interacts with CDC42 and functions as a GTPase activating protein (GAP), thereby inhibiting CDC42 activity and subsequent filopodia formation. Furthermore, we have discovered that Akt phosphorylates Rbsn at the Thr253 site, and this phosphorylation negates the inhibitory effect of Rbsn on CDC42 activity. Additionally, our analysis reveals that Rbsn expression is significantly downregulated in lung cancer, and this decrease is associated with a worse prognosis. These findings provide strong evidence supporting the role of Rbsn in suppressing lung cancer progression through the inhibition of metastasis.

Cancer Gene Therapy (2024) 31:1465–1476; <https://doi.org/10.1038/s41417-024-00813-4>

BACKGROUND

Non-small cell lung cancer (NSCLC) represents a grave concern for public health, leading the spectrum of malignancies in both incidence and mortality [1, 2]. Due to the significant advancements in targeted therapy and immunotherapy in recent years, the survival of NSCLC patients has improved [3]. Nevertheless, a substantial subset of patients is diagnosed at an advanced stage, with metastases already present [4]. The metastasis of lung cancer impacts the quality of life of patients, and results in the leading cause of death [5, 6]. Consequently, an in-depth exploration of the molecular mechanisms underlying NSCLC metastasis is imperative. This research is pivotal for identifying novel therapeutic targets and developing innovative pharmacological strategies, thereby enhancing treatment outcomes for patients with NSCLC.

Cytoskeletal remodeling is a pivotal process in cancer cell metastasis, with small Rho GTPases acting as key regulators. Among these, Rac, cell division cycle protein 42 (CDC42), and Rho are extensively characterized for their distinct roles in cytoskeletal dynamics. Rac activation is associated with the generation of lamellipodia and membrane ruffles, CDC42 activation promotes filopodia assembly, and Rho activation is linked to the formation of stress fibers [7, 8]. These small Rho GTPases have garnered attention as critical targets in anticancer therapy due to their central roles in modulating cytoskeletal dynamics, which is fundamental to cancer metastasis. They facilitate metastatic spread by not only driving the migratory and invasive capabilities of cancer cells [9–11] but also by

augmenting the migration of endothelial cells, a process essential for angiogenesis [12–14].

Rho GTPase proteins exhibit activity when localized at the plasma membrane or endomembrane (e.g., endosomes, Golgi) [15]. The intracellular trafficking of these proteins plays a crucial role in their cellular functions by influencing their subcellular distribution. For instance, Arf6-mediated membrane trafficking can modulate the localization and activation of CDC42, thereby impacting CDC42-driven cell migration [16]. Additionally, Rab5, a key regulator of endocytosis, has been shown to activate Rac and promote lamellipodia formation by facilitating the trafficking of Rac to the cell membrane [17]. Furthermore, Rab5 has been implicated in integrin trafficking [18], cytoskeleton remodeling [19], and cell metastasis [20–22]. Notably, the downregulation of Rab5 has been observed to inhibit the activity of small Rho GTPases, leading to a suppression of filopodia and lamellipodia formation [23]. Currently, these findings revealed membrane trafficking regulatory proteins modulate small Rho GTPase activity via intercellular trafficking pathways. Generally, small Rho GTPase activity can be directly regulated by GTPase Activating Protein (GAP) and Guanine Exchange Factor (GEF), it is unknown whether membrane trafficking regulatory proteins can directly interact with and regulate small Rho GTPase activity.

Rabenosyn-5 (Rbsn) serves as an effector for the small Rab GTPases Rab4 and Rab5, orchestrating their function as elucidated in prior research [24–26]. The role of Rbsn in the endocytic

¹Department of Colorectal and Anal Surgery, Xiangya Hospital, Central South University, 410008 Changsha, China. ²Shanghai Zhaohui Pharmaceutical Co. Ltd, 200436 Shanghai, China. ³Department of Biochemistry and Molecular Biology, Shenyang Medical College, 113004 Shenyang, China. ⁴Key laboratory of Human Ethnic Specificity and Phenomics of Critical Illness in Liaoning Province, Shenyang Medical College, 113004 Shenyang, China. ⁵Department of drug inspection (II), Shenyang Institute for Food and Drug Control, 110000 Shenyang, China. ⁶Department of Physiology, Shenyang Medical College, 113004 Shenyang, China. ⁷Department of Anatomy, Shenyang Medical College, 113004 Shenyang, China. ⁸Department of Pharmaceutical Analysis, Shenyang Medical College, 113004 Shenyang, China. ⁹Shenyang Key Laboratory for Screening Biomarkers of Tumor Progression and Targeted Therapy of Tumors, Shenyang Medical College, 113004 Shenyang, China. ✉email: pingmu@sycm.edu.cn; rfs@sycm.edu.cn; lufangjin@sycm.edu.cn

Received: 7 January 2024 Revised: 5 July 2024 Accepted: 18 July 2024
Published online: 29 July 2024

pathway is well-established, where it governs the trafficking of a plethora of internalized receptors, including but not limited to the transferrin receptor, major histocompatibility complex class I, and the epidermal growth factor receptor (EGFR) [26–28]. Beyond receptor trafficking, Rbsn is implicated in the preservation of microtubule polarity and modulating the subcellular distribution of intracellular RNA [29]. In *Drosophila*, Rbsn is indispensable for the biogenesis of early endosomes in the context of vesicular fusion, as evidenced by one investigation [30]. Disruption of Rbsn function leads to compromised epithelial polarity and aberrant tissue proliferation, culminating in tumorigenesis [30]. Despite these insights, the involvement of Rbsn in tumor metastasis and its capacity to modulate small Rho GTPase activity remain enigmatic. There is a pressing need for further inquiry to unravel the role of Rbsn in these critical processes and to ascertain its potential as a modulatory agent of small Rho GTPase-mediated signaling.

In this study, we observed a downregulation of Rbsn in NSCLC compared to normal lung tissue and demonstrated its ability to suppress filopodia formation and lung cancer metastasis by inhibiting the GTPase activity of CDC42. Interestingly, we found that this process is regulated by the phosphorylation of the Rbsn Thr253 site, mediated by Akt. Therefore, our findings reveal a novel mechanism by which Rbsn regulates cell migration and invasion through function as a GAP for small Rho GTPases, thereby impacting lung cancer metastasis.

METHODS

Plasmid construction and antibodies

The retrovirus-based Flag-Rbsn expressing plasmid was generated by flanking PCR fragment of human Rbsn cDNA and synthesizing 3xFlag sequence, then inserted into a pRetroQ-AcGFP-C1 vector (Clontech, San Jose, CA, USA) using BamHI and EcoRI, and NheI and BglIII respectively. The retrovirus-based SF (StreptII-Flag)-Rbsn expressing plasmid for tandem affinity purification (TAP) experiment was generated by flanking PCR fragment of human Rbsn cDNA, then inserted into pMXs-SF (StreptII-Flag) vector using EcoRI and NotI. Akt1 was cloned from 293 T cell cDNA via PCR and inserted into the pLVx-HA vector. To simulate the kinase active state (DA), the S473D mutation (Akt1 S473D forward: 5'-ccgtggccgagtagtc-gaactgggggaagtg-3'; reverse: 5'-cacttccccagctgactactcgccagcgg-3'), and the kinase-dead mutant K179M (Akt1 K179M forward: 5'-ctctctcttgag-gatcatcatggcgtagtagcgg-3'; reverse: 5'-ccgtactacgcatgatgatctcaagaag-gaag-3') were introduced. The primers corresponding to these mutations were used to amplify pLVx-HA-Akt1. The pLVx-HA-Akt1 plasmid was then digested with DpnI enzyme to remove the template plasmid. Subsequently, the constructs were transformed into BI21-competent cells for plasmid extraction.

The following antibodies were employed: anti-Flag (clone M2, Sigma, St. Louis, Missouri, USA), anti-Rbsn (sc-82729, Santa Cruz Biotechnology, Dallas, Texas, USA), anti- β -actin (clone AC-74, Sigma), anti-CDC42 (ACD03, Cytoskeleton, Denver, CO, USA), anti-Rac1 (ARC03, Cytoskeleton), anti-Rho (ARH04, Cytoskeleton), anti-Akt (CST#9272, Cell Signaling Technology, Denver, CO, USA), anti-phospho-Akt (Ser473) (CST #4060, Cell Signaling Technology), and anti-phospho Akt substrate (RXXS*/T*) (CST #9614, Cell Signaling Technology).

Cell culture and establish stable cell lines by retrovirus infection

A549, H1299, and 293T cells used in this study were obtained from the American Type Culture Collection (ATCC). BEAS-2B cells used in this study were obtained from the National Collection of Authenticated Cell Cultures (Shanghai, China). A549 cell line was cultured in Roswell Park Memorial Institute (RPMI) 1640 (RPMI 1640, Gibco, Carlsbad, CA, USA). H1299, BEAS-2B and 293T cell lines were cultured in Dulbecco's Modified Eagle Medium (DMEM, Gibco) supplemented with 10% fetal bovine serum (FBS, Sigma-Aldrich) and 1% penicillin-streptomycin (Gibco) in a humidified atmosphere containing 5% CO₂ at 37 °C.

The retrovirus plasmids (24 μ g) and 4 μ g of vesicular stomatitis virus G protein (pVSV-G) vector (Clontech Laboratories, Palo Alto, CA, USA) were introduced into GP2-293 packaging cells (Clontech Laboratories). After

24 h, the medium was replaced with 5 mL of fresh DMEM supplemented with 10% FBS. The supernatants containing the viral particles were collected 48 h post-transfection and subsequently used to infect the target cells. The infected cells were then subjected to selection with 2 μ g/mL puromycin.

For the transient transfection of 293T cells, the cells were seeded into 6 cm dishes and allowed to adhere and grow until they reached the logarithmic phase of growth. The plasmids were mixed with the transfection reagent Lipo8000 (C0533, Beyotime Biotechnology, Shanghai, China) at a mass-to-volume ratio of 1:2 in 200 μ l of basic DMEM medium, and this mixture was then added dropwise to the cell culture medium. Protein was extracted 48 h later.

Co-immunoprecipitation and Western blotting analysis

Cells were lysed in immunoprecipitation lysis buffer (20 mM Tris-HCl, 120 mM NaCl, 0.8% Triton X100, 1 mM EDTA, pH 7.4) supplemented with protease inhibitors Cocktail (Selleck, Houston, TX, USA). The supernatants were then incubated with 1 μ g of primary antibody or control IgG at 4 °C overnight. Following this, 20 μ l of protein A/G sepharose beads (Thermo Fisher Scientific, Waltham, MA, USA) were added and incubated at 4 °C for 3 h. The beads were subsequently washed with immunoprecipitation lysis buffer, and the protein complex was eluted using 100 μ l of SDS sample buffer.

To investigate the interaction between Rbsn and CDC42, cells were lysed with GTPase immunoprecipitation buffer (20 mM Tris-HCl, 120 mM NaCl, 1 mM EDTA, 0.8% Triton X-100, 5 mM MgCl₂, pH 7.4). All of the Mg²⁺ in each 500 μ l of cell lysate were chelated with 7.5 μ l of 0.5 M EDTA (pH 8.0). Subsequently, 5 μ l of 0.5 M Guanosine-5'-(γ -thio)-triphosphate (GTP γ S, a non-hydrolyzable GTP analog which can create constitutively GTP bound GTPases) or GDP (final concentration, 0.5 mM) was added to the lysate and incubated for 15 min at room temperature to load GTP γ S or GDP. Following this, 30 μ l of 1 M MgCl₂ was added to the lysate to stabilize the binding of the nucleotide to the dynamin GTPase. The primary antibody was then added and incubated for 3 h, followed by the addition of protein A/G sepharose beads for another 3 h. The protein complex was eluted using 100 μ l of SDS sample buffer.

Western blotting was performed as previously described [31]. Briefly, the protein sample was prepared and separated by sodium dodecyl sulfate-polyacrylamide gel electrophoresis (SDS-PAGE). After the separation, the protein was transferred from the gel to polyvinylidene difluoride (PVDF) membranes (GE Healthcare, Marlborough, MA, USA). The membrane was then blocked with 5% dry milk in phosphate-buffered saline (PBS) for 1 h at room temperature and was then incubated with the indicated primary antibody at 4 °C overnight. After 3 times washing, the membrane was incubated with horseradish peroxidase-conjugated secondary antibodies (Jackson ImmunoResearch, West Grove, PA, USA) at room temperature for 1 h, followed by 3 times PBS washing. After washing, the ECL reagent (GE Healthcare) was added to the membrane and the images were taken.

Small Rho GTPase activity assay

The activation of small Rho GTPase activity was performed with the RhoA/Rac1/CDC42 activation assay combo biochem kit (Cytoskeleton) according to the manufacturer's instructions. Briefly, 40 μ l of the specific affinity beads targeting RhoA, Rac1, and CDC42 were added to the 1 mL of cell lysate in assay lysis buffer and were incubated at 4 °C for 1 h. The active form of small Rho GTPase was pulled down in the bead pellet by centrifugation for 10 s at 14,000 \times g. The supernatant was discarded, and the bead pellet was washed 3 times with 0.5 mL of assay buffer. After the last wash, the bead pellet was mixed with 40 μ l of SDS-PAGE sample buffer and was boiled for 5 min. After the centrifugation, the supernatant was used to perform Western blotting with the specific antibody targeting RhoA, Rac1, or CDC42.

To assess the GTPase activity of CDC42, a malachite green-based colorimetric assay was conducted following previously described methods [32]. Briefly, the purified proteins were mixed as the indicated molar ratio in a diluting buffer for 30 min. Then the GTPase assay buffer (12.5 mM NaCl, 2.5 mM MgCl₂, 0.0625% Tween-80, 1.25 μ g/mL of leupeptin, 125 μ M PMSF, 375 μ M GTP, 15 mM Tris-HCl, pH 7.4) was added to 96-well plates, followed with the addition of the protein mixture. The samples were incubated at 30 °C with continuous shaking at a rate of 300 rpm, and the reaction was terminated by adding 0.5 M EDTA at the indicated time. The samples were treated with 150 μ l of malachite green reagent and developed the color. The absorption spectra at 650 nm were measured.

Tandem affinity purification (TAP) of protein complex

To purify Rbsn-interacting proteins, H1299 cells stably expressing SF (StrepII-Flag dual tag)-Flag or SF-Rbsn were established after the infection with indicated plasmid and were selected with 2 µg/mL puromycin. To extract the proteins, 5 × 15 cm dishes of each cell were lysed using immunoprecipitation lysis buffer (20 mM Tris-HCl, 120 mM NaCl, 1 mM EDTA, 0.8% Triton X-100, 5 mM MgCl₂, pH 7.4) and then incubated with 200 µl of Strep-Tactin superflow resin from IBA LifeSciences (Louvain-La-Neuve, Belgium) for 6 h at 4 °C. After washing with lysis buffer 3 times, the protein complex was eluted by employing 1 mL of elution buffer#1 (Tris-buffered saline (TBS) buffer containing 2 mM Desthiobiotin from IBA). Following this, the eluate was subjected to the second round of purification by incubating with 100 µl anti-Flag resin overnight at 4 °C. After washing with lysis buffer 3 times, the protein complex was subsequently eluted using elution buffer#2 (TBS buffer containing 200 µg/mL of Flag peptide from Sigma). Then 20 µl samples were loaded for SDS-PAGE and visualized by silver staining using The Pierce Silver Stain Kit (#24612, Thermo Fisher Scientific).

Identify Rbsn-interacting proteins by mass spectrometry analysis

For the identification of proteins included in the tandem affinity purification eluate, the whole eluates were digested with Trypsin Gold (Promega, Madison, WI) for 16 h at 37 °C after reduction, alkylation, demineralization and concentration, followed by analysis on the Orbitrap Fusion mass spectrometer (Thermo Fisher Scientific). The protein-protein interaction network was generated by STRING (<https://cn.string-db.org/>).

CCK8 assay

Cells were seeded in 96-well plates at a density of 2000 cells per well and allowed to adhere overnight. The medium was then removed, and 20 µl of Cell Counting Kit-8 (CCK-8) solution along with 200 µl of medium was added to each well. The plates were incubated for an additional 1 h at 37 °C. Absorbance at 450 nm was measured using a microplate reader to determine cell viability. CCK-8 measurements were taken every 24 h. Each treatment was performed in triplicate, and data were normalized to control wells containing medium without the test compound. Results were expressed as mean ± SD. Statistical significance was assessed using Student's *t*-test.

Wound healing assay

A549 or H1299 cells were seeded in 6-well plates at a density of 5 × 10⁵ cells per well and allowed to adhere for 24 h to achieve a confluent monolayer. A wound was introduced to the monolayer using a 200 µl pipette tip, ensuring consistent wound width. Following scratch application, wells were gently washed twice with PBS to remove cellular debris and floating cells. The cells were then incubated in basic RPMI 1640 or DMEM to minimize proliferation. Images of the same field were taken immediately after wounding and again after 24 h using a microscope. The wound closure ratio was calculated using the formula: (Wound area at 0 h - Wound area at 24 h) / Wound area at 0 h * 100%. The experiment was repeated three times and data were presented as mean ± SD. Statistical significance was assessed using Student's *t* test.

Transwell assay

For invasion assays, 8.0 µm pore size Transwell inserts (Corning, NY, USA) were coated with Matrigel (diluted to 1 mg/mL, incubated overnight at 4 °C) to mimic the extracellular matrix; no coating was used for migration assays. Cells were seeded at a density of 5 × 10⁴ cells/mL in the basic medium into the upper chamber, with a medium containing 20% FBS in the lower chamber. After incubating for 24 h, cells that migrated or invaded the lower side of the membrane were fixed with 4% formaldehyde for 20 min and stained with 0.1% crystal violet for 30 min. Images of the stained cells were captured using a Leica microscope, and the cells were quantified using ImageJ software. The experiment was repeated three times and data were presented as mean ± SD. Statistical significance was assessed using Student's *t*-test.

Immunofluorescence staining

The cells were washed with PBS 3 times and then were fixed with 4% paraformaldehyde for 15 min at room temperature. The cells were

incubated at 0.1% Triton X-100 in PBS at room temperature for 10 min. After washing with PBS 3 times, the cells were incubated with the indicated primary antibody overnight at 4 °C, followed by washing with PBS 3 times. Then the cells were incubated with the appropriate fluorochrome-conjugated secondary antibody (Invitrogen, Carlsbad, CA, USA) for 1 h at room temperature. After washing with PBS, the cells were incubated with DAPI for 10 min at room temperature and were mounted with Fluoroshield (sigma). Images were captured using a Leica SP8-DMIL confocal microscope with a 63 x oil objective lens. For each group, 100 cells were randomly selected and assessed for the presence of prominent filopodia. Each experiment was repeated three times. Statistical analysis was performed using the Student's *t*-test.

Immunohistochemistry

Tissues were fixed in 4% paraformaldehyde, dehydrated, and embedded in paraffin according to the standard procedure. The tissues were cut into 5-µm-thick sections and were blocked with 5% goat serum for 1 h at room temperature. The sections were then treated with the indicated primary antibody in 5% goat serum overnight at 4 °C and were washed in PBS 3 times. Then sections were subsequently incubated with the second antibody for 1 h at room temperature. After being washed in PBS, the slides were developed with 3, 3'-diaminobenzidine and images were taken.

Animal experiment

2 × 10⁶ H1299 cells in 100 µL of PBS were injected into the tail veins of 6-8 weeks female BALB/c nude mice (Liaoning Changsheng Biotechnology, Benxi, Liaoning, China), with 6 mice used per group, and the groups were completely randomized. No blinding was done. Eight weeks after injection, the mice were sacrificed and the tumor burden was checked in the lung through hematoxylin-eosin staining (HE) staining. In this study, all animal experiments were conducted in strict adherence to the ethical principles outlined in the Declaration of Helsinki. We ensured that all experimental procedures were aimed at minimizing pain and discomfort to the animals and were carried out in strict compliance with relevant national and international guidelines and regulations. The experimental protocols were reviewed and approved by the Laboratory Animal Ethics Committee of Xiangya Hospital (approval #202110138).

Clinical samples

Non-small cell lung cancer samples were collected from the Department of Pathology, Xiangya Hospital. A total of 95 NSCLC patients, excluded receive any treatment before surgery, were selected. The expression of Rbsn in the lung cancer sample and adjacent para-cancerous sample were examined. This study was approved by the Clinical Research Ethics Committee of Xiangya Hospital (approval #2021101149). Patient details are shown in Table 1. Researchers blinded the clinical information of patients before analyzing the data. Statistical significance was assessed using the Chi-square test. A *p*-value of less than 0.05 was considered statistically significant.

Statistical analysis

Data are presented as mean ± standard error (SE). Statistical significance between two groups was assessed using a two-tailed Student's *t* test. For comparisons involving more than two groups, one-way ANOVA was employed. In instances where the data involved two independent factors, two-way ANOVA was utilized to evaluate the main effects and the interactions between these factors. Overall survival rates were estimated using the Kaplan-Meier method, with statistical comparisons conducted using the Log-rank test. A *p*-value of less than 0.05 was considered statistically significant.

RESULTS

Low expression of Rbsn is correlated with poor prognosis of NSCLC patients

To discern the clinical relevance of Rabenosyn-5 (Rbsn) in non-small cell lung cancer (NSCLC), we embarked on an initial exploration of NSCLC patient datasets. This preliminary analysis disclosed a diminution of Rbsn expression in NSCLC specimens relative to non-cancerous lung tissue (Fig. 1A, S1A, and S1B).

Notably, this downregulation correlated with a decline in overall patient survival (Fig. 1B). To corroborate these observations, we assessed Rbsn levels across a spectrum of lung cancer cell lines and compared them with the human normal lung epithelial cell line BEAS-2B (Fig. 1C). Consistently, Rbsn expression was found to be lower in the most lung cancer cell lines than that in the BEAS-2B cells (Fig. 1C). Subsequent immunohistochemical analyses of NSCLC tissues, sourced from patients undergoing surgical intervention at Xiangya Hospital, further substantiated the reduced expression of Rbsn in tumor cells (Fig. 1D, E). This diminished expression was again linked to poorer overall survival outcomes (Fig. 1F). Moreover, a significant relationship was observed between Rbsn expression levels, the incidence of lymph node

metastasis, and the TNM staging in NSCLC patients (Table 1). The expression of Rbsn in patients was found to be independent of age, gender, and tumor size. Besides, patients with high Rbsn expression exhibited a lower rate of lymph node metastasis and were more likely to be in the early stages of tumor development. In aggregate, these data intimate that Rbsn may serve as an inhibitory factor in the progression and metastatic behavior of NSCLC.

Rbsn inhibits lung cancer cell migration and invasion

To delineate the contribution of Rbsn to NSCLC pathobiology, we engineered A549 and H1299 cell lines to stably overexpress Rbsn. Intriguingly, Rbsn upregulation did not markedly impact the proliferation of these NSCLC cell lines, as indicated by Cell Counting Kit-8 (CCK8) assay outcomes (Fig. 2A). Similarly, the capacity for anchorage-independent growth remained unchanged following Rbsn enhancement (Fig. 2B, C). Conversely, a pronounced attenuation of migratory and invasive capabilities was observed in cells overexpressing Rbsn, as evidenced by wound healing (Fig. 2D, E) and transwell assays (Fig. 2F, G). These data collectively imply that Rbsn principally impedes NSCLC progression by thwarting the migratory and invasive potential of lung cancer cells.

Rbsn inhibits CDC42 activity

To elucidate the mechanistic basis for Rbsn-mediated suppression of cancer cell migration and invasion, we examined the small Rho GTPase signaling pathway, a pivotal modulator of cytoskeletal organization. Employing assays to measure the activity of Rac, CDC42, and Rho, we discovered a significant reduction in active CDC42 in the Flag-Rbsn-expressing cells relative to the empty vector (EV) controls, while levels of active Rac1 and Rho remained unaltered between the two groups (Fig. 3A–D, S2A, and S2B). This suggests that Rbsn overexpression selectively downregulates CDC42 activity without affecting Rac and Rho pathways. Complementing these findings, we noted a decrease in filopodia

Table 1. The Rbsn expression in NSCLC patients.

Variable		All patients (n = 95)	High expression Total n = 47 n (%)	Low expression Total n = 48 n (%)	p
Gender	Male	55	26 (55.3)	29 (60.4)	0.4705
	Female	40	21 (44.7)	19 (39.6)	
Age (years)	<60	47	26 (55.3)	21 (43.8)	0.1121
	≥60	48	21 (44.7)	27 (56.2)	
Tumor size	T1-2	68	33 (70.2)	35 (72.9)	0.6619
	T3-4	27	14 (29.8)	13 (27.1)	
Lymph node metastasis	N0-1	61	35 (74.5)	26 (54.2)	0.0056
	N2	34	12 (25.5)	22 (45.8)	
TNM stage	I-II	67	40 (85.1)	27 (56.2)	0.0001
	III-IV	28	7 (14.9)	21 (43.8)	

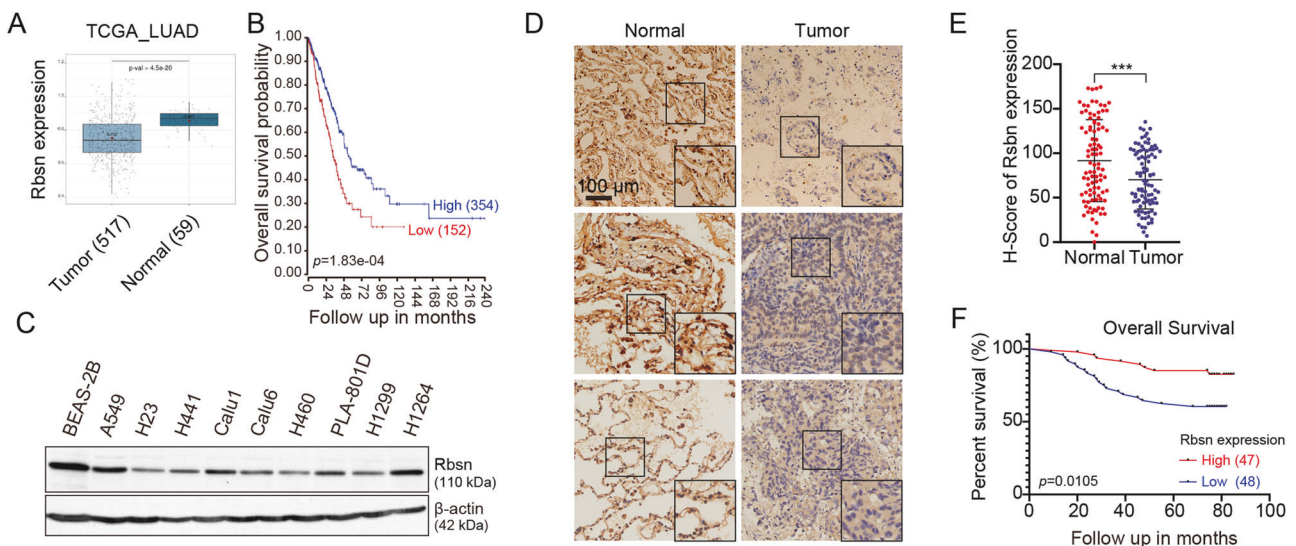


Fig. 1 Rbsn is lowly expressed in NSCLC. **A** The expression of Rbsn in NSCLC patients was analyzed in the LUNG CANCER EXPLORER platform (TCGA_LUAD_2016 dataset). The numbers in parentheses represent the sample size. A two-tailed Student's *t*-test was used for statistical analyses. **B** Kaplan–Meier analysis of prognosis about Rbsn expression in NSCLC patients from an R2 clinic patient database (TCGA-515-rsem-tcgars dataset). Rbsn expression levels were divided into high and low groups based on the median expression level of Rbsn. Log-rank test was used for statistical analyses. **C** The expression of Rbsn was assessed in different cell lines using Western blotting. **D, E** Immunohistochemical staining of Rbsn was performed in human NSCLC tissues. The right panels in **(D)** show a higher magnification of the regions within the black boxes. The quantification results of Rbsn staining are presented in **(E)**. A two-tailed Student's *t* test was used for statistical analyses. Data are presented as means \pm SE ($n = 95$), $***p < 0.001$. **F** Overall survival analysis was conducted to evaluate the impact of Rbsn expression on NSCLC patients. Rbsn expression levels were divided into high and low groups based on the median expression level of Rbsn. Log-rank test was used for statistical analyses.

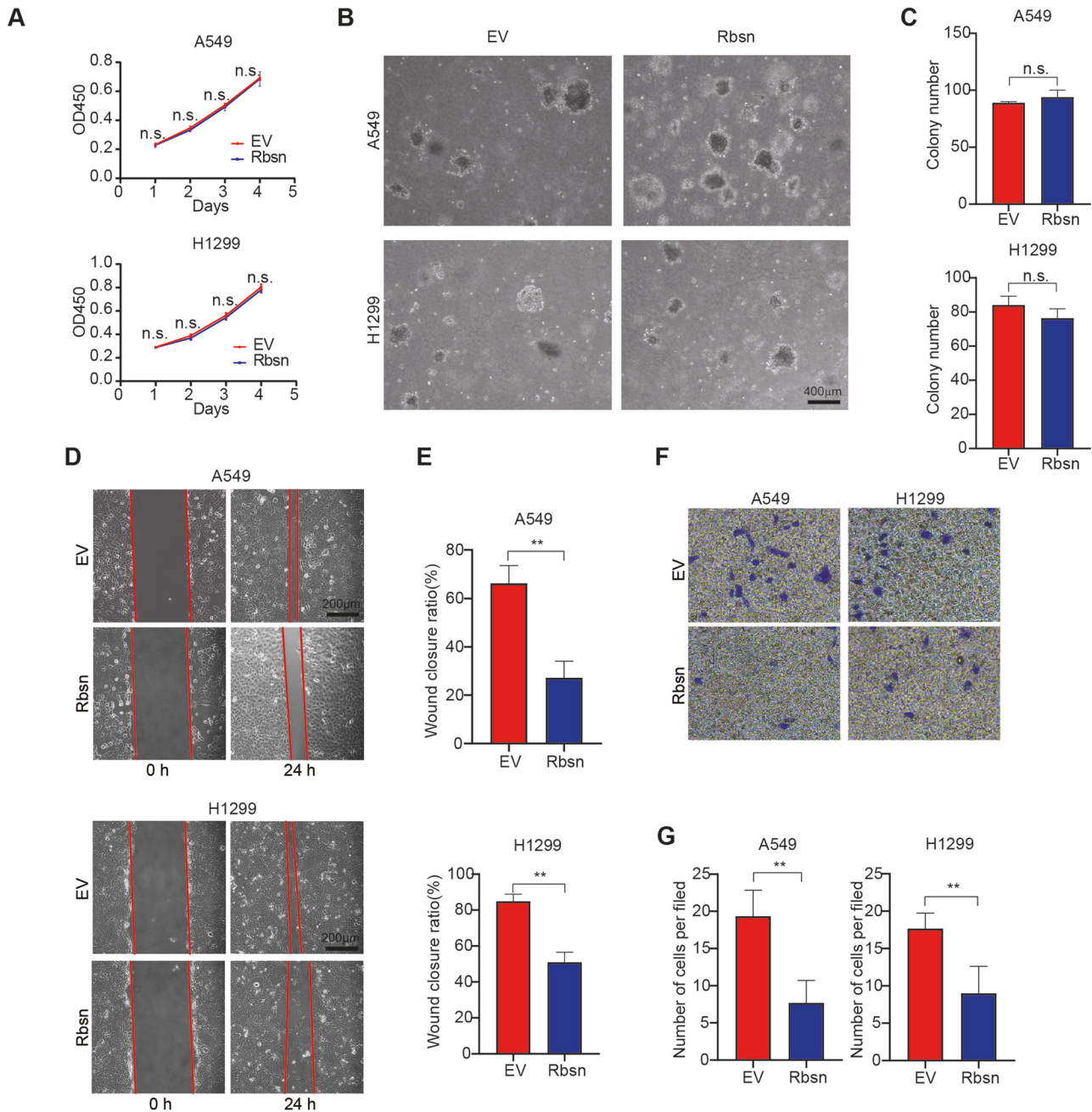


Fig. 2 Rbsn inhibits lung cancer cell migration and invasion. **A** The effect of Rbsn on the proliferation of lung cancer cells was examined using CCK8 analysis ($n = 3$, technical replicates) and the experiments were conducted with at least three independent repetitions. **B, C** The colony formation of lung cancer cells in soft agar was assessed, with or without Rbsn overexpression. The quantification data are shown in **(C)** ($n = 3$, technical replicates) and the experiments were conducted with at least three independent repetitions. **D, E** Lung cancer cell migration was evaluated using a wound healing assay, with or without Rbsn overexpression. The quantification data are shown in **(E)** ($n = 3$, technical replicates) and the experiments were conducted with at least three independent repetitions. **F, G** The invasion of lung cancer cells was examined using a transwell assay, with or without Rbsn overexpression. The quantification data are shown in **(G)** ($n = 3$, technical replicates) and the experiments were conducted with at least three independent repetitions. In the results of **(A)**, **(C)**, **(E)**, and **(G)**, a two-tailed Student's t test was used for statistical analyses. Data are presented as means \pm SE, ** $p < 0.01$. EV indicates empty vector; n.s. indicates no significant difference.

formation, a cellular process governed by CDC42, in both A549 (Fig. 3E, G) and H1299 cells (Fig. 3F, H) overexpressing Rbsn. These findings suggest that Rbsn impedes cancer cell motility and invasiveness by specifically targeting and inhibiting CDC42 activity.

Rbsn is a GTPase-activating protein (GAP) for CDC42

To delineate the regulatory influence of Rbsn on CDC42 activity, we employed tandem affinity purification (TAP) to isolate Rbsn-

associated proteins from H1299 cell lysates. Extracts from cells expressing either EV or SF-tagged Rbsn underwent TAP, with the resultant protein complexes visualized by silver staining and subjected to mass spectrometric identification (Fig. 4A). Remarkably, CDC42 emerged as a prominent member of the Rbsn interaction network (Fig. S3). Co-immunoprecipitation assays further corroborated the Rbsn-CDC42 interaction in A549 and H1299 cells (Fig. 4B, C). Additionally, Rbsn

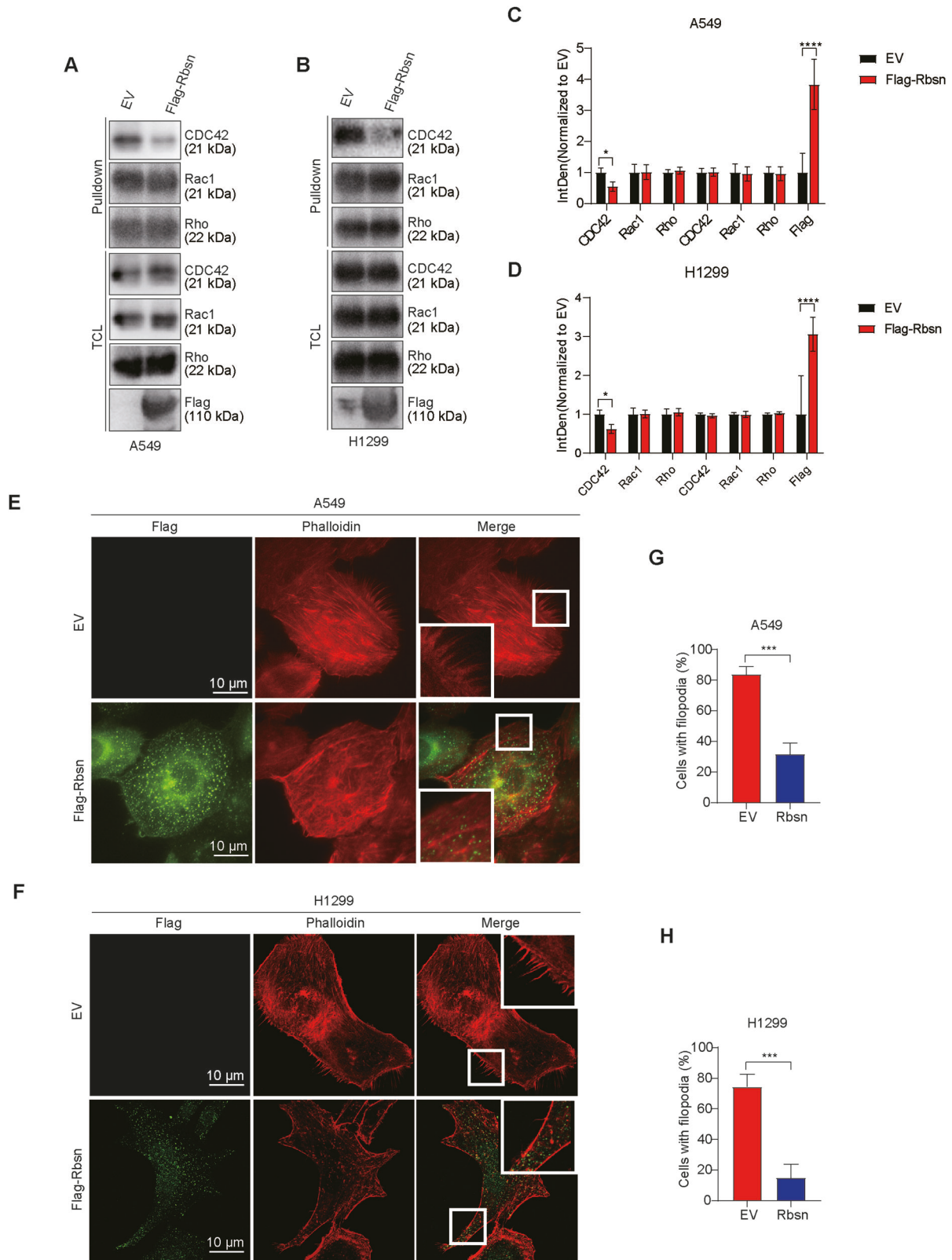


Fig. 3 Rbsn inhibits CDC42 activity. **A–D** The GTPase activity of CDC42, Rac1, and Rho in lung cancer cells, both with and without Rbsn overexpression, was assessed through repeated experiments using a small Rho GTPase activity assay, along with the statistical analysis related to A549 (**C**) and H1299 (**D**). **E–H** Cells were infected with indicated plasmids, and immunofluorescence was performed 72 h later to visualize filopodia formation in lung cancer cells with or without Rbsn overexpression. Closed boxes are magnified in the insets. The percentage of cells with filopodia in each group (100 cells from three independent experiments) is quantified in (**G**) and (**H**), respectively. Two-tailed Student's *t* test was used for statistical analyses. Data are presented as means \pm SE, * $p < 0.05$, *** $p < 0.001$, **** $p < 0.0001$. EV indicates empty vector; TCL indicates total cell lysate.

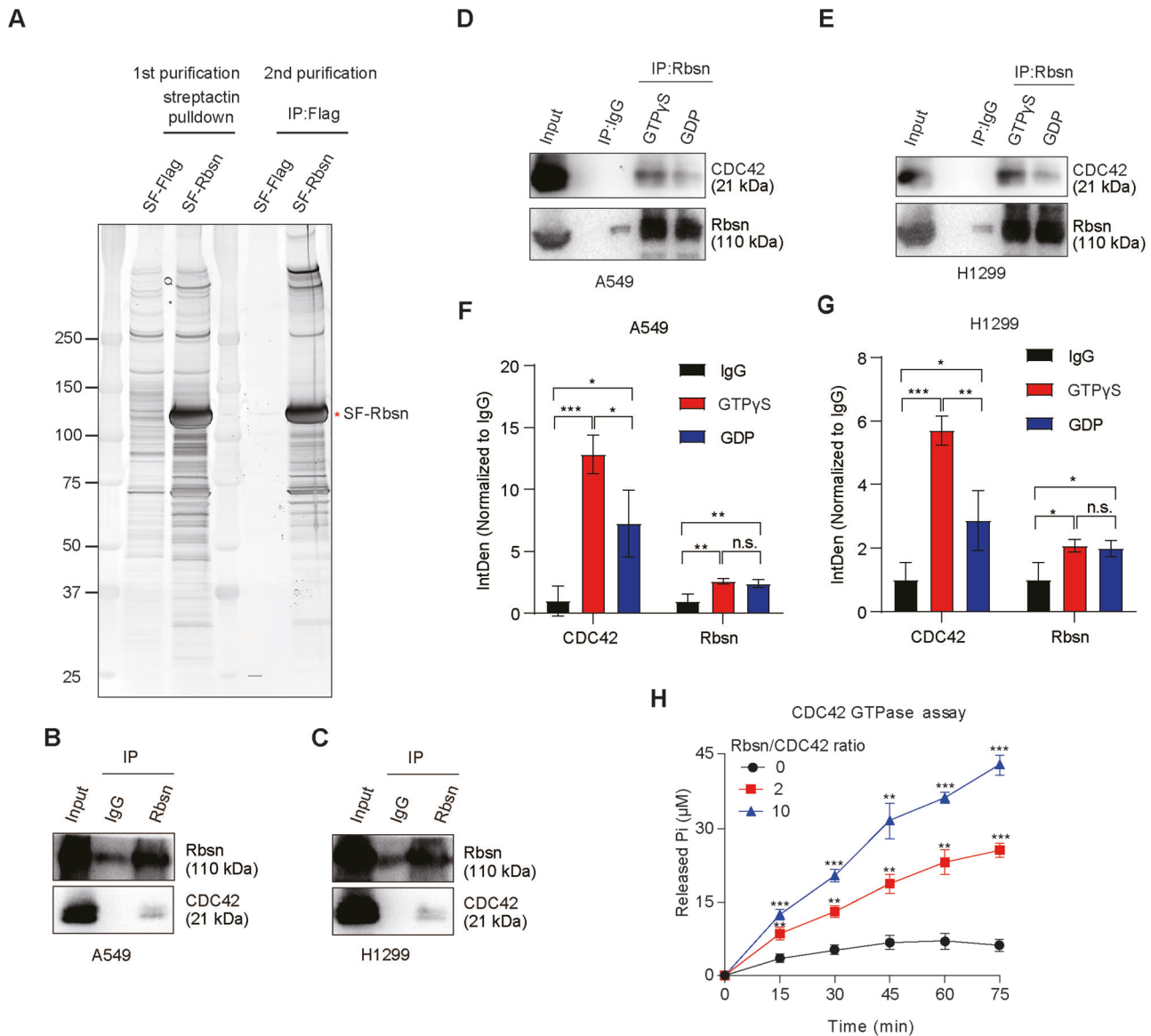
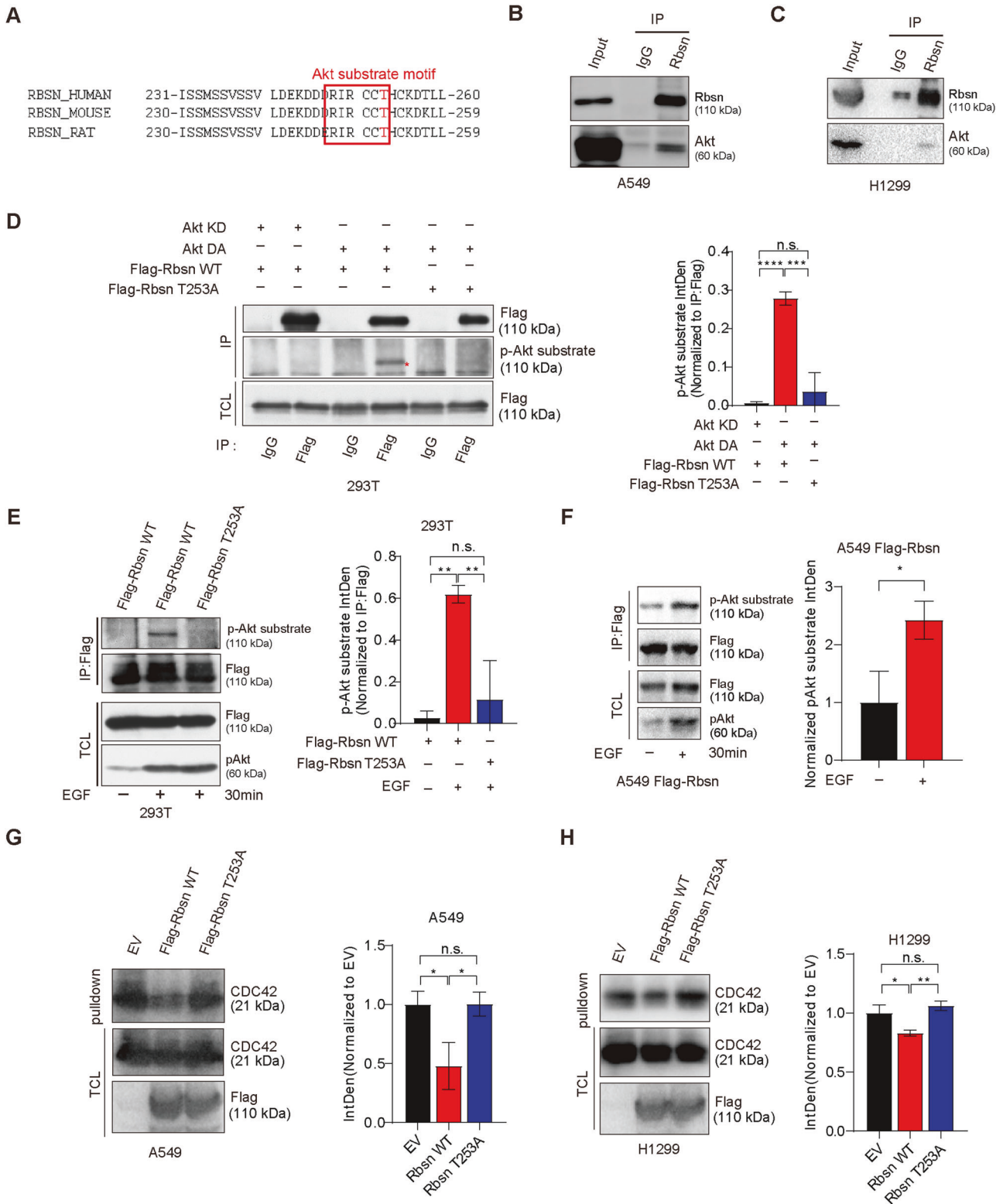


Fig. 4 Rbsn is a GAP for CDC42. **A** Tandem affinity purification was performed to isolate the Rbsn interacting proteins in H1299 cells, followed by visualization of the protein complex using silver staining. **B, C** The interaction between endogenous Rbsn and CDC42 was examined by co-immunoprecipitation in A549 (**B**) and H1299 (**C**). **D–G** The interaction between endogenous Rbsn and CDC42 was examined by co-immunoprecipitation in the presence of either GTP γ S or GDP, along with the statistical analysis related to A549 (**F**) and H1299 (**G**), a two-way ANOVA was used for statistical analyses. **H** CDC42 GTPase activity assays were conducted to assess the impact of the Rbsn on CDC42 GTPase activity. The results demonstrated that the Rbsn increased CDC42 GTPase activity in a time- and dose-dependent manner. The numbers represent the molar ratio of the Rbsn protein to the CDC42 protein utilized in this assay. A one-way ANOVA test was used for statistical analyses. Data are presented as means \pm SE ($n = 6$, technical replicates) and the experiments were conducted with at least three independent repetitions, * $p < 0.05$, ** $p < 0.01$, *** $p < 0.001$. IP indicates immunoprecipitation.

demonstrated a binding preference for the GTP-bound form of CDC42 when in the presence of non-hydrolyzable GTP γ S, but not with GDP (Fig. 4D–G). This specificity suggests a direct interaction between Rbsn and the active state of CDC42. Subsequent colorimetric GTPase assays, varying both the temporal and molar parameters of Rbsn and CDC42, indicated that Rbsn potentiates the GTPase activity of CDC42 in a time- and dose-dependent fashion (Fig. 4H). Moreover, knocking down Rbsn in A549 and H1299 cells was observed to enhance the activity of CDC42 (Fig. S4A–B). These findings strongly implicate Rbsn as a GAP for CDC42, enhancing the conversion of GTP to GDP and thereby attenuating CDC42 activity.

Akt-induced Rbsn Thr253 phosphorylation regulates GAP activity of Rbsn

To investigate the regulatory mechanisms of Rbsn GAP activity, we scrutinized the amino acid sequence of Rbsn, noting that a threonine residue at position 253 resides within conserved Akt phosphorylation motifs (R-x-R-x-x-5/T) (Fig. 5A). Moreover, we found that the interaction between Rbsn and Akt occurs in A549 and H1299 cells respectively, as demonstrated by co-immunoprecipitation assays (Fig. 5B, C). To determine whether Akt phosphorylates Rbsn at Thr253, 293T cells were co-transfected with vectors expressing either constitutively active Akt (Akt DA) or kinase-dead Akt (Akt KD) along with a Flag-Rbsn



vector. Immunoprecipitation using an anti-Flag antibody, followed by detection with an anti-phospho Akt substrate (RXXS*/T*) antibody, revealed that Akt DA facilitated phosphorylation of wild-type Rbsn, whereas Akt KD did not (Fig. 5D). Mutation of Rbsn at Thr253 to alanine (T253A) abrogated its phosphorylation, pinpointing Thr253 as the specific Akt

phosphorylation site (Fig. 5D). Epidermal growth factor (EGF) stimulation, which activates Akt, induced phosphorylation of wild-type Rbsn in 293 T cells but not the T253A mutant, further validating Thr253 as the target (Fig. 5E). Simultaneously, EGF also stimulated the activation of Rbsn in A549 cells (Fig. 5F). Functional assays revealed that overexpression of wild-type

Fig. 5 Akt-induced Rbsn phosphorylation is essential for CDC42 activity regulation. **A** Amino acid sequences of Rbsn from various species are presented, with the conserved threonine at position 253 (highlighted in red) conforming to the Akt substrate motif. **B, C** The endogenous interaction between Rbsn and Akt was checked by co-immunoprecipitation in lung cancer cells. **D** Indicated plasmids were transfected into 293T cells, and the immunoprecipitation was performed with anti-Flag antibody or control IgG, followed by p-Akt substrate to check the phosphorylation of Rbsn, along with statistical analysis of three independent experiments. A One-way ANOVA was used for statistical analyses. **E, F** The indicated plasmids were transfected into 293 T cells (**E**), or A549 Flag-Rbsn cell line (**F**) stimulated with or without 100 ng/ml EGF for 30 min. Subsequently, the immunoprecipitation was performed with anti-Flag antibody or control IgG. The phosphorylated Rbsn was examined with a p-Akt substrate, along with statistical analysis of three independent experiments. A One-way ANOVA and two-tailed Student's *t* test was used for statistical analyses. **G, H** CDC42 activity assay to examine CDC42 activity in lung cancer cells stably expressing with indicated plasmids. The active CDC42 was purified by a pull-down experiment with the affinity beads, along with statistical analysis of three independent experiments. A One-way ANOVA was used for statistical analyses. WT indicates wild type; IP indicates immunoprecipitation; TCL indicates total cell lysate. Data are presented as means \pm SE, **p* < 0.05, ***p* < 0.01, ****p* < 0.001, *****p* < 0.0001.

Rbsn attenuated CDC42 activity in A549 and H1299 cells, as assessed by pull-down assays using CDC42 affinity beads. This inhibitory effect was not observed with the Rbsn T253A mutant (Fig. 5G, H). Moreover, the Rbsn T253A mutation negated the effects on filopodia formation (Fig. 6A, B), cell migration (Fig. 6C, D), and invasion (Fig. 6E, F). These results collectively underscore the pivotal role of Akt-mediated phosphorylation of Rbsn at Thr253 in modulating its GAP activity toward CDC42, with downstream consequences on cancer cell morphology, motility, and invasive behavior.

Rbsn inhibits lung cancer metastasis in vivo

To validate the impact of Rbsn on lung cancer metastasis in an in vivo setting, H1299 cells were intravenously injected into immunocompromised nude mice (Fig. 7A). After 8 weeks, the mice were sacrificed, and their lungs were collected for assessment of tumor burden. Notably, the overexpression of wild-type Rbsn led to a significant reduction in lung metastasis compared to the EV control cells. Conversely, the overexpression of the Rbsn T253A mutant showed minimal impact on metastasis, similar to that observed in the EV control group (Fig. 7B, C). These findings provide further evidence supporting the inhibitory role of Rbsn in lung cancer metastasis.

DISCUSSION

Metastatic dissemination is the leading cause of mortality in cancer patients. Proteins involved in intracellular trafficking have emerged as pivotal modulators of cytoskeletal dynamics. In this study, we have elucidated that the expression level of Rbsn is markedly reduced in NSCLC, correlating with a poorer patient prognosis. Our data further demonstrate that Rbsn functions as a GAP for the small GTPase CDC42, thereby attenuating CDC42-mediated signaling pathways that drive filopodia assembly and, consequently, tumor cell metastasis. Moreover, we have identified a critical post-translational modification; specifically, phosphorylation of Rbsn at threonine 253 by Akt kinase is requisite for its GAP activity, underscoring a novel regulatory mechanism of Rbsn function in cancer progression.

CDC42, a pivotal member of the Rho GTPase family, toggles between an active GTP-bound state and an inactive GDP-bound state. The regulation of small Rho GTPase activity is principally orchestrated by GEFs and GAPs. GEFs facilitate the transition to the active GTP-bound conformation, thereby stimulating small Rho GTPase activity, whereas GAPs expedite GTP hydrolysis, effectively terminating the signaling [33]. Specific mutations in CDC42, such as G12V and Q61L, have been shown to compromise GTPase hydrolytic function, resulting in aberrant cellular morphology [34]. In contrast, the F28L mutation enhances the dynamic interconversion between GDP- and GTP-bound states [35], culminating in filopodia formation [36]. Dysregulation of small

Rho GTPase signaling, as evidenced in various neoplasms, underscores the importance of modulating GTPase activity in the context of tumorigenesis [37].

The functional diversity of CDC42 GAPs in key biological processes is well-documented. SrGAPs, a subset of CDC42 GAPs, have been implicated in the regulation of Slit-mediated neuronal migration [38, 39]. In *Saccharomyces cerevisiae*, the CDC42 GAP Rga1 influences the establishment of polarity axis orientation, asymmetric cell division, and longevity, with Rga1-deficient yeast displaying a reduced lifespan due to compromised polarity establishment [40, 41]. Conversely, Rga3 appears to be non-essential for cell polarization during mitotic growth in yeast [42]. Rga4 has been identified as a determinant of growth patterns across successive generations [43]. In *Schizosaccharomyces pombe*, Rga6 regulates the septin complex's cortical localization, thereby controlling monopolar growth during spore germination; loss of Rga6 results in aberrant bipolar growth due to impaired septin localization [44]. The involvement of CDC42 GAPs in oncogenesis has also been explored. CdGAP, a CDC42-specific GAP, is upregulated following TGF- β stimulation and participates in TGF- β -mediated migration and invasion of breast cancer cells [45]. Furthermore, CdGAP modulates gene expression associated with epithelial-mesenchymal transition (EMT) [46], influences cancer cell migration and invasion [47], and is implicated in VEGF-dependent angiogenesis [48]. Despite the critical functions of CDC42 GAPs elucidated in various studies, the repertoire of known GAPs remains comparatively small against the backdrop of identified GEFs.

Previous studies have primarily centered on its role as an effector of the small Rab GTPases Rab4 and Rab5, orchestrating endocytic trafficking pathways with implications for diseases such as congenital neutrophil defect syndrome and intractable seizures [49, 50]. Furthermore, Rab5A has been implicated in promoting Rbsn-dependent endo/exocytic cycles, which are critical for protein degradation and the invasive capacity of tumors, potentially enhancing metastatic progression [51]. In addition, previous studies revealed intracellular trafficking proteins modulate small Rho GTPases activity via regulating their intracellular trafficking [52, 53]. However, our study has revealed for the first time that Rbsn functions as a GAP of small Rho GTPase CDC42 and can directly inhibit the activity of CDC42 through its GAP function. This discovery sheds light on the crosstalk between small Rab GTPases and small Rho GTPases, suggesting that intracellular trafficking may regulate the functions of small Rho GTPases.

Our study also has some limitations. A notable limitation is the absence of a specific antibody targeting the Thr253 phosphorylation site on Rbsn, which precluded the analysis of phosphorylated Rbsn within tumor specimens. Additionally, the possibility of phosphorylation at alternative sites on Rbsn and the consequent effects on its regulatory activity warrant further exploration.

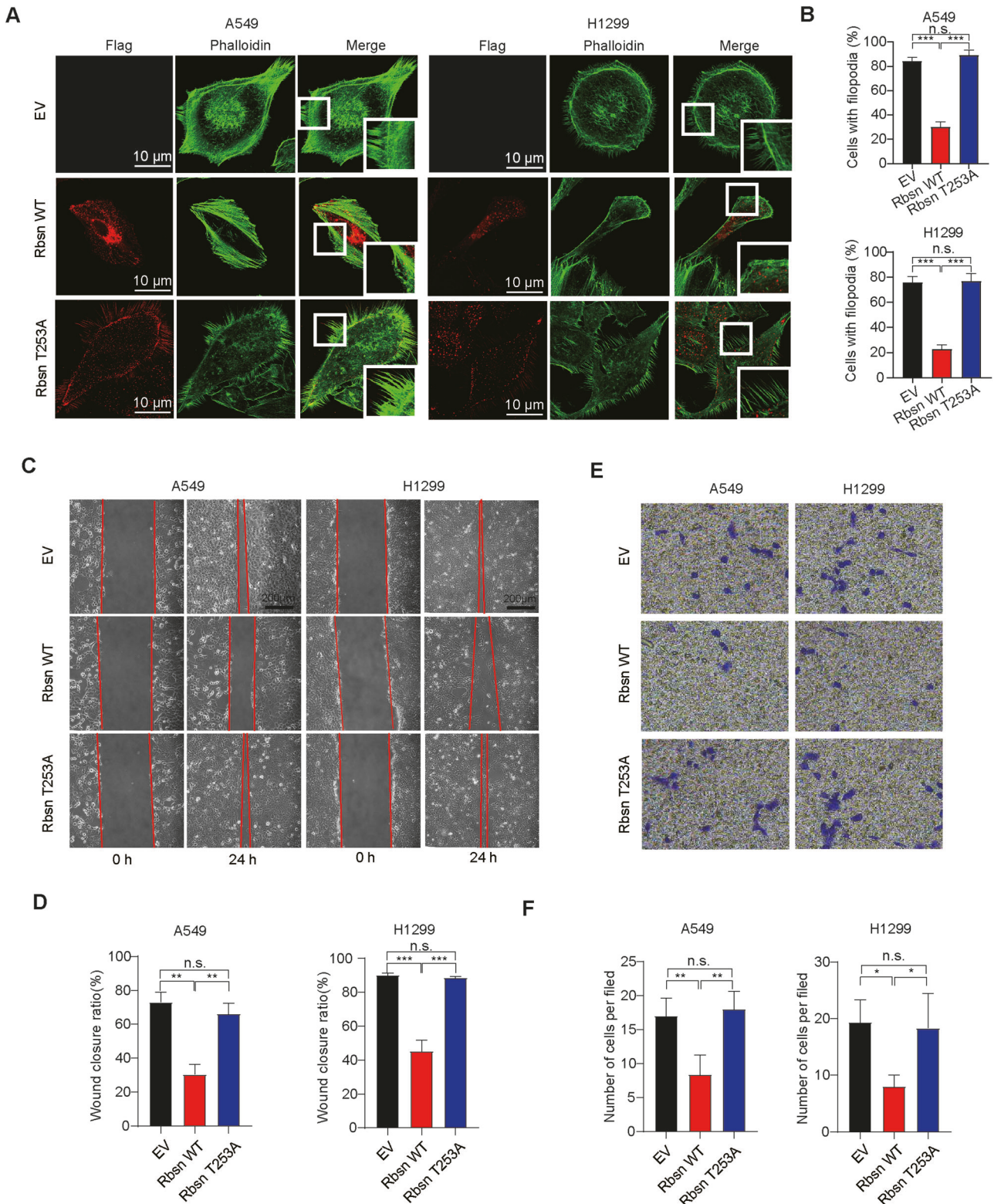


Fig. 6 Rbsn Thr253 phosphorylation is essential for lung cancer cell migration and invasion. **A, B** Cells were infected with indicated plasmids, and immunofluorescence was performed 72 h later to visualize filopodia formation in lung cancer cells expressing the indicated plasmids. Closed boxes in **(A)** are magnified in the insets. The percentage of cells with filopodia in each group (100 cells from three independent experiments) is quantified in **(B)**, and a One-way ANOVA was used for statistical analyses. **C, D** Wound healing assay to examine cell migration in lung cancer cells stably expressing with indicated plasmids. The quantification data from three independent experiments are shown in **(D)** ($n = 3$, technical replicates) and the experiments were conducted with at least three independent repetitions. **E, F** Cell invasion in lung cancer cells expressing the indicated plasmids was examined using a transwell assay. Quantification data for cell invasion are presented in **(F)** ($n = 3$, technical replicates) and the experiments were conducted with at least three independent repetitions. In the results of **(B)**, **(D)**, and **(F)**, a One-way ANOVA was used for statistical analyses. Data are presented as means \pm SE, * $p < 0.05$, ** $p < 0.01$, *** $p < 0.001$. EV indicates an empty vector; WT indicates wild type.

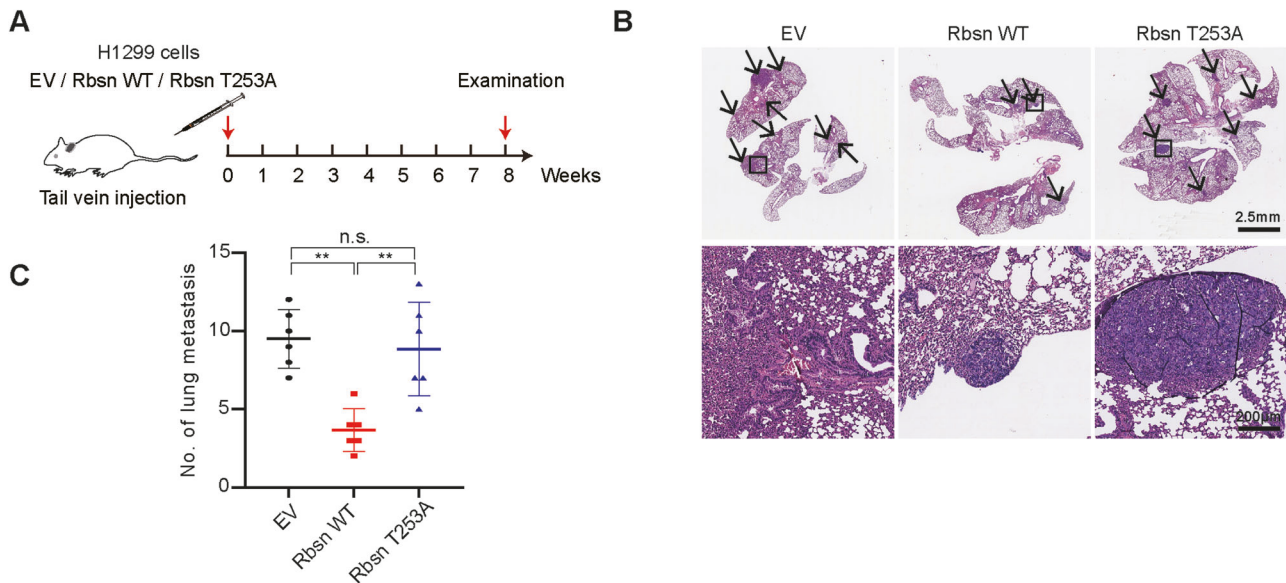


Fig. 7 Rbsn inhibits lung cancer metastasis in vivo. **A** Schematic of the mice models to check lung cancer metastasis. **B, C** Representative images depicting the metastatic tumor foci in the lungs are presented. Quantification data for the number of metastatic tumor foci are shown in **(C)**. A One-way ANOVA was used for statistical analyses. Data are presented as means \pm SE (6 mice per group), $**p < 0.01$. EV indicates an empty vector; WT indicates wild type.

CONCLUSIONS

Our work demonstrates that Rbsn suppresses lung cancer metastasis by reducing CDC42 activity.

DATA AVAILABILITY

The clinical patient dataset generated and analyzed during the current study is available in the Gene Expression Profiling Interactive Analysis platform (<http://gepia.cancer-pku.cn>) and R2 clinic patient database platform (<http://hgserver1.amc.nl/cgi-bin/r2/main.cgi>), respectively.

REFERENCES

- Vachani A, Sequist LV, Spira A. Ajrcm: 100-year anniversary. The shifting landscape for lung cancer: past, present, and future. *Am J Respir Crit Care Med*. 2017;195:1150–60.
- Goldstraw P, Ball D, Jett JR, Le Chevalier T, Lim E, Nicholson AG, et al. Non-small-cell lung cancer. *Lancet*. 2011;378:1727–40.
- Hirsch FR, Scagliotti GV, Mulshine JL, Kwon R, Curran WJ Jr, Wu YL, et al. Lung cancer: current therapies and new targeted treatments. *Lancet*. 2017;389:299–311.
- Relli V, Trerotola M, Guerra E, Alberti S. Abandoning the notion of non-small cell lung cancer. *Trends Mol Med*. 2019;25:585–94.
- Planchard D, Popat S, Kerr K, Novello S, Smit EF, Faivre-Finn C, et al. Metastatic non-small cell lung cancer: ESMO Clinical Practice Guidelines for diagnosis, treatment and follow-up. *Ann Oncol*. 2018;29:iv192–iv237.
- Donnem T, Kilvaer TK, Andersen S, Richardsen E, Paulsen EE, Hald SM, et al. Strategies for clinical implementation of TNM-Immunoscore in resected nonsmall-cell lung cancer. *Ann Oncol*. 2016;27:225–32.
- Nobes CD, Hall A. Rho, rac, and cdc42 GTPases regulate the assembly of multi-molecular focal complexes associated with actin stress fibers, lamellipodia, and filopodia. *Cell*. 1995;81:53–62.
- Hall A. Rho GTPases and the actin cytoskeleton. *Science*. 1998;279:509–14.
- Zhou HC, Liu CX, Pan WD, Shang LR, Zheng JL, Huang BY, et al. Dual and opposing roles of the androgen receptor in VETC-dependent and invasion-dependent metastasis of hepatocellular carcinoma. *J Hepatol*. 2021;75:900–11.
- Guo Y, Zhu J, Wang X, Li R, Jiang K, Chen S, et al. Orai1 promotes osteosarcoma metastasis by activating the ras-rac1-wave2 signaling pathway. *Med Sci Monit*. 2019;25:9227–36.
- Yang W, Wu PF, Ma JX, Liao MJ, Xu LS, Yi L. Trpv4 activates the cdc42/n-wasp pathway to promote glioblastoma invasion by altering cellular protrusions. *Sci Rep*. 2020;10:14151.

- Khan S, Shukla S, Farhan M, Sinha S, Lakra AD, Penta D, et al. Centchroman prevents metastatic colonization of breast cancer cells and disrupts angiogenesis via inhibition of rac1/pak1/beta-catenin signaling axis. *Life Sci*. 2020;256:117976.
- Barbera S, Lugano R, Pedalina A, Mongiat M, Santucci A, Tosi GM, et al. The c-type lectin CD93 controls endothelial cell migration via activation of the rho family of small GTPases. *Matrix Biol*. 2021;99:1–17.
- Sakabe M, Fan J, Odaka Y, Liu N, Hassan A, Duan X, et al. Yap/Taz-CDC42 signaling regulates vascular tip cell migration. *Proc Natl Acad Sci USA*. 2017;114:10918–23.
- Phuyal S, Farhan H. Multifaceted Rho GTPase signaling at the endomembranes. *Front Cell Dev Biol*. 2019;7:127.
- Osmani N, Peglion F, Chavrier P, Etienne-Manneville S. Cdc42 localization and cell polarity depend on membrane traffic. *J Cell Biol*. 2010;191:1261–9.
- Palamidessi A, Frittoli E, Garre M, Faretta M, Mione M, Testa I, et al. Endocytic trafficking of rac is required for the spatial restriction of signaling in cell migration. *Cell*. 2008;134:135–47.
- Pellinen T, Arjonen A, Vuoriluoto K, Kallio K, Fransén JA, Ivaska J. Small GTPase rab21 regulates cell adhesion and controls endosomal traffic of beta1-integrins. *J Cell Biol*. 2006;173:767–80.
- Lanzetti L, Palamidessi A, Areces L, Scita G, Di Fiore PP. Rab5 is a signalling GTPase involved in actin remodelling by receptor tyrosine kinases. *Nature*. 2004;429:309–14.
- Torres VA, Mielgo A, Barbero S, Hsiao R, Wilkins JA, Stupack DG. Rab5 mediates caspase-8-promoted cell motility and metastasis. *Mol Biol Cell*. 2010;21:369–76.
- Yang PS, Yin PH, Tseng LM, Yang CH, Hsu CY, Lee MY, et al. Rab5a is associated with axillary lymph node metastasis in breast cancer patients. *Cancer Sci*. 2011;102:2172–8.
- Shen D, Lin J, Xie Y, Zhuang Z, Xu G, Peng S, et al. RNA demethylase alkhh5 promotes colorectal cancer progression by posttranscriptional activation of Rab5a in an m6A-ythdf2-dependent manner. *Clin Transl Med*. 2023;13:e1279.
- Liu SS, Chen XM, Zheng HX, Shi SL, Li Y. Knockdown of rab5a expression decreases cancer cell motility and invasion through integrin-mediated signaling pathway. *J Biomed Sci*. 2011;18:58.
- Nielsen E, Christoforidis S, Uttenweiler-Joseph S, Miaczynska M, Dewitte F, Wilm M, et al. Rabenosyn-5, a novel rab5 effector, is complexed with hvp5 45 and recruited to endosomes through a fyve finger domain. *J Cell Biol*. 2000;151:601–12.
- Eathiraj S, Pan X, Ritacco C, Lambright DG. Structural basis of family-wide rab GTPase recognition by rabenosyn-5. *Nature*. 2005;436:415–9.
- De Renzis S, Sonnichsen B, Zerial M. Divalent rab effectors regulate the sub-compartmental organization and sorting of early endosomes. *Nat Cell Biol*. 2002;4:124–33.
- Naslavsky N, Boehm M, Backlund PS Jr, Caplan S. Rabenosyn-5 and ehd1 interact and sequentially regulate protein recycling to the plasma membrane. *Mol Biol Cell*. 2004;15:2410–22.

28. Navaroli DM, Bellvé KD, Standley C, Lifshitz LM, Cardia J, Lambright D, et al. Rabenosyn-5 defines the fate of the transferrin receptor following clathrin-mediated endocytosis. *Proc Natl Acad Sci USA*. 2012;109:E471–E780.
29. Tanaka T, Nakamura A. The endocytic pathway acts downstream of oskar in drosophila germ plasm assembly. *Development*. 2008;135:1107–17.
30. Morrison HA, Dionne H, Rusten TE, Brech A, Fisher WW, Pfeiffer BD, et al. Regulation of early endosomal entry by the drosophila tumor suppressors rabenosyn and vps45. *Mol Biol Cell*. 2008;19:4167–76.
31. Lu F, Mu B, Jin G, Zhu L, Mu P. Mycn directly targets neuroD1 to promote cellular proliferation in neuroblastoma. *Oncol Res*. 2022;29:1–10.
32. Weng L, Enomoto A, Miyoshi H, Takahashi K, Asai N, Morone N, et al. Regulation of cargo-selective endocytosis by dynamin 2 GTPase-activating protein girdin. *EMBO J*. 2014;33:2098–112.
33. Qiu RG, Abo A, McCormick F, Symons M. Cdc42 regulates anchorage-independent growth and is necessary for ras transformation. *Mol Cell Biol*. 1997;17:3449–58.
34. Miller PJ, Johnson DI. Cdc42p GTPase is involved in controlling polarized cell growth in *Schizosaccharomyces pombe*. *Mol Cell Biol*. 1994;14:1075–83.
35. Lin R, Bagrodia S, Miyoshi H, Takahashi K, Asai N, Morone N, et al. Regulation of cargo-selective endocytosis by dynamin 2 GTPase-activating protein girdin. *EMBO J*. 2014;33:2098–112.
36. Aspenstrom P. The intrinsic GDP/GTP exchange activities of Cdc42 and rac1 are critical determinants for their specific effects on mobilization of the actin filament system. *Cells*. 2019;8:759.
37. Vigil D, Cherfils J, Rossman KL, Der CJ. Ras superfamily GEFs and GAPs: validated and tractable targets for cancer therapy? *Nat Rev Cancer*. 2010;10:842–57.
38. Zhu Y, Li H, Zhou L, Wu JY, Rao Y. Cellular and molecular guidance of GABAergic neuronal migration from an extracortical origin to the neocortex. *Neuron*. 1999;23:473–85.
39. Wong K, Ren XR, Huang YZ, Xie Y, Liu G, Saito H, et al. Signal transduction in neuronal migration: roles of GTPase activating proteins and the small GTPase Cdc42 in the slit-robo pathway. *Cell*. 2001;107:209–21.
40. Kang PJ, Mullner R, Li H, Hansford D, Shen HW, Park HO. Up-regulation of the cdc42 GTPase limits the replicative life span of budding yeast. *Mol Biol Cell*. 2022;33:br5.
41. Miller KE, Lo WC, Lee ME, Kang PJ, Park HO. Fine-tuning the orientation of the polarity axis by rga1, a Cdc42 GTPase-activating protein. *Mol Biol Cell*. 2017;28:3773–88.
42. Gallo Castro D, Martin SG. Differential GAP requirement for Cdc42-GTP polarization during proliferation and sexual reproduction. *J Cell Biol*. 2018;217:4215–29.
43. Pino MR, Nuñez I, Chen C, Das ME, Wiley DJ, D'Urso G, et al. Cdc42 GTPase-activating proteins (GAPs) regulate generational inheritance of cell polarity and cell shape in fission yeast. *Mol Biol Cell*. 2021;32:ar14.
44. Zheng S, Zheng B, Liu Z, Ma X, Liu X, Yao X, et al. The Cdc42 GTPase-activating protein rga6 promotes the cortical localization of septin. *J Cell Sci*. 2022;135:jcs259228.
45. He Y, Northey JJ, Primeau M, Machado RD, Trembath R, Siegel PM, et al. CdGAP is required for transforming growth factor beta- and neu/erbb-2-induced breast cancer cell motility and invasion. *Oncogene*. 2011;30:1032–45.
46. He Y, Northey JJ, Pelletier A, Kos Z, Meunier L, Haibe-Kains B, et al. The Cdc42/rac1 regulator CdGAP is a novel e-cadherin transcriptional co-repressor with zeb2 in breast cancer. *Oncogene*. 2017;36:3490–503.
47. Wormer D, Deakin NO, Turner CE. CdGAP regulates cell migration and adhesion dynamics in two- and three-dimensional matrix environments. *Cytoskeleton (Hoboken)*. 2012;69:644–58.
48. Caron C, DeGeer J, Fournier P, Duquette PM, Luangrath V, Ishii H, et al. CdGAP/ arhgap31, a Cdc42/rac1 GTPase regulator, is critical for vascular development and vegf-mediated angiogenesis. *Sci Rep*. 2016;6:27485.
49. Vilboux T, Lev A, Malicdan MC, Simon AJ, Järvinen P, Racek T, et al. A congenital neutrophil defect syndrome associated with mutations in vps45. *N. Engl J Med*. 2013;369:54–65.
50. Stockler S, Corvera S, Lambright D, Fogarty K, Nosova E, Leonard D, et al. Single point mutation in rabenosyn-5 in a female with intractable seizures and evidence of defective endocytotic trafficking. *Orphanet J Rare Dis*. 2014;9:141.
51. Frittoli E, Palamidessi A, Marighetti P, Confalonieri S, Bianchi F, Malinverno C, et al. A rab5/rab4 recycling circuitry induces a proteolytic invasive program and promotes tumor dissemination. *J Cell Biol*. 2014;206:307–28.
52. Stenmark H. Rab GTPases as coordinators of vesicle traffic. *Nat Rev Mol Cell Biol*. 2009;10:513–25.
53. El Masri R, Delon J. RHO GTPases: from new partners to complex immune syndromes. *Nat Rev Immunol*. 2021;21:499–513.

ACKNOWLEDGEMENTS

The authors gratefully thank L. Weng (Central South University) for providing the pMXs-SF (StreptI-Flag) vector, constitutively active human Akt expressing vector (Akt DA), and dominant-negative human Akt expressing vector (Akt KD).

AUTHOR CONTRIBUTIONS

FL, FR, and PM designed experiments, guided research, and revised manuscripts. XG performed the experiments, analyzed data, and wrote the manuscript. LZ and YZ performed the experiments and analyzed the data. BM supervised and planned research. All authors have read and agreed to the published version of the manuscript.

FUNDING

This work was funded by Liaoning Provincial Natural Science Foundation of China (2020-MS-309, 2022-NLTS-14-04 to FL), the Foundation of the Central Government Guides Local Science and Technology Development Fund (2023JH6/100100021 to FR), the Foundation of the Education Department of Liaoning Province of China (LJKM20221787 to PM), the Foundation of Spring Sunshine Program-Cooperative Research Project of the Ministry of Education (202200846 to PM), and Hunan Provincial Natural Science Foundation of China (2022JJ30364 to XG).

COMPETING INTERESTS

The authors declare no competing interests.

ETHICS APPROVAL AND CONSENT TO PARTICIPATE

The study was approved by the Ethics Committee of Xiangya Hospital (approval #2021101149), and conducted in accordance with the Helsinki Declaration of 1975. Written informed consent was obtained from all subjects involved in the study. The experimental procedures with animals were approved by the Laboratory Animal Ethics Committee of Xiangya Hospital (approval #202110138), and all experiments were performed following the guidelines for ethical review of animal welfare of laboratory animals, designated by the Ministry of Science and Technology of China (2018).

ADDITIONAL INFORMATION

Supplementary information The online version contains supplementary material available at <https://doi.org/10.1038/s41417-024-00813-4>.

Correspondence and requests for materials should be addressed to Ping Mu, Fu Ren or Fangjin Lu.

Reprints and permission information is available at <http://www.nature.com/reprints>

Publisher's note Springer Nature remains neutral with regard to jurisdictional claims in published maps and institutional affiliations.



Open Access This article is licensed under a Creative Commons Attribution-NonCommercial-NoDerivatives 4.0 International License, which permits any non-commercial use, sharing, distribution and reproduction in any medium or format, as long as you give appropriate credit to the original author(s) and the source, and provide a link to the Creative Commons license. You do not have permission under this license to share adapted material derived from this article or parts of it. The images or other third party material in this article are included in the article's Creative Commons license, unless indicated otherwise in a credit line to the material. If material is not included in the article's Creative Commons license and your intended use is not permitted by statutory regulation or exceeds the permitted use, you will need to obtain permission directly from the copyright holder. To view a copy of this license, visit <http://creativecommons.org/licenses/by-nc-nd/4.0/>.